the square of the quoted errors. These are shown in Table II, together with the values obtained by other workers for comparison.

Bondelid's values are very closely similar to the values which we obtained relative to the 340.4-kev resonance determination and are consequently approximately one part in a thousand lower than our best mean values. The constancy of the discrepancy is consistent with both scales being linear to a few parts in ten thousand.

Comparison with Bumiller and Staub's results shows that their values are $0.6/10^3$ lower than ours for the lowest energy and about $0.8/10^3$ lower at the higher energies, but $2.6/10^3$ lower for intermediate energies. This is not consistent with both scales being accurately linear.

The agreement between our mean values and Herb's values in the medium energy range is good to two parts in ten thousand.

ACKNOWLEDGMENTS

The authors would like to thank Dr. R. H. Thomas and Mr. G. Hunt, who assisted in the experimental work, members of the Laboratory workshop staff who were responsible for the machining of the electrostatic analyzer and Mr. E. Fellows who was responsible for much of the electronic circuitry in the ± 50 kv voltage supply. The continued interest and encouragement of Dr. D. R. Chick is gratefully acknowledged and thanks are also due to Dr. T. E. Allibone, F.R.S., Director of the Laboratory, for permission to publish this paper.

PHYSICAL REVIEW VOLUME 120, NUMBER 5 DECEMBER 1, 1960

Energy Loss and Effective Charge of Heavy Ions in Aluminum*

L. C. NORTHCLIFFE
Yale University, New Haven, Connecticut

(Received March 22, 1960; revised manuscript received September 1, 1960)

Heavy-ion beams of fixed initial energy ($E^0/m \approx 10$ Mev/amu) are passed through aluminum absorbers of known thickness, and the emergent ions are analyzed by means of a magnetic spectrograph to determine their charge and energy distributions. Accurate measurements of the mean emergent ion energy as a function of absorber thickness are reported for beams of He^4, B^{10}, B^{11}, C^{12}, N^{14}, O^{16}, F^{19}, and Ne^{20} ions with emergent energies in the range $10 > E/m > 1$ Mev/amu. The results can be interpreted as measurements of the range-energy relation for heavy ions. While the absolute accuracy of the range measurements is approximately ± 1 mg/cm^2, the range difference $R(E^0) - R(E)$ is measured (as a function of E) with a typical accuracy of ± 0.1 mg/cm^2. In the analysis the shape of the heavy-ion range-energy curve is compared with the accurately known shape of the proton range-energy curve (using the conversion factor $\Delta R = mZ_p^2(m_pZ^2)^{-1}\Delta R_p$) and the differences in shape are attributed to deviations of the effective charge of the ion from its nuclear charge. No detectable difference is found between the shape of the range-energy curve for He^4 ions and for protons. For heavier ions, deviations in the curve shape do occur. A simple empirical formula is found for the effective charge of an ion as a function of its velocity which is consistent with the deviations of the observed range-energy curves and presumably can be used to predict the range-energy curves for ions not investigated experimentally. By an independent analysis of the spectrograph data the equilibrium distribution of charge states in the O^{16} beam is determined as a function of emergent beam energy. The effective charge implied by the charge state distribution is found to be consistent with the effective charge as given by the empirical formula.

I. INTRODUCTION

A. Background

ALTHOUGH the penetration of energetic charged particles through a material medium has been the subject of widespread theoretical and experimental investigation for more than forty years,[1] the phenomenon is of such complexity that it generally has not been possible to predict the behavior of a particular type of particle in a given absorbing medium with precision on the basis of theory alone, or even from the behavior of other ions in other media. Experimental measurements have been necessary, not only for each combination of incident ion species and absorbing material, but for different regions of incident ion energy as well. The case of aluminum is of particular importance as well as being illustrative, since it often is regarded as the standard absorbing material. The range-energy relation for α particles in aluminum was investigated with high precision in the energy region up to 10 Mev, the highest energy available with natural α sources.[2] Yet there is a difference of 5% between the predictions for the range of a 40-Mev α particle given in two different collections of range-energy relations[3,4]

* This work was supported by the U. S. Atomic Energy Commission. A preliminary report was given in Bull. Am. Phys. Soc. 4, 44 (1959).

[1] Extensive bibliographies and discussions of the available information from various viewpoints are given in references 3, 4, and 23, and by S. K. Allison and S. D. Warshaw, Revs. Modern Phys. 25, 779 (1953).

[2] S. Rosenblum, Ann. Physik 10, 408 (1928).

[3] W. Whaling, *Encyclopedia of Physics* (Springer-Verlag, Berlin, Germany, 1958), Vol. 34, p. 210.

[4] W. A. Aron, B. G. Hoffman, and F. C. Williams, Atomic Energy Commission Report AECU-663, May, 1951 (unpublished).

currently in wide use. A similar uncertainty in the range-energy relation for high-energy protons in aluminum was reduced only recently by the precise experiments of Bischsel, Mozley, and Aron[5] and of Bichsel.[6] The situation with regard to heavier ions is even more uncertain because the theoretical predictions are complicated by the partial neutralization of the ions as they lose energy,[7–14] and the amount of published experimental information for ions with energies in excess of 1 Mev per nucleon has been very limited.[15–19] The recent development of heavy-ion accelerators and the current interest in reactions involving energetic heavy ions have increased the need for accurate knowledge of the heavy-ion range-energy relations. This information is needed not only for the many different heavy-ion beams which can be produced by accelerators but also for the large variety of energetic ions (most of which are short-lived) which can be formed as reaction products. When the number of absorbing materials of interest is considered, it can be seen that the total number of ion-absorber combinations is very large. Therefore, it is desirable not only that range-energy measurements be made with the greatest possible efficiency but also that methods be found for predicting the results with ion-absorber combinations which have not been studied. In addition, the range-energy results should have high absolute accuracy if they are to be useful in the determination of the energy of an ion by measurement of its range.

The work reported here was undertaken in order to help fill this need.[20] The equipment is designed so as to make possible the rapid accumulation of complete and accurate data on the energy loss process for a variety of beams and absorbing materials. Energy loss results in aluminum absorbing material are presented[21] for ions of He^4, B^{10}, B^{11}, C^{12}, N^{14}, O^{16}, F^{19}, and Ne^{20} with incident energies of approximately 10 Mev per nucleon; emergent energies in the range from 10 to 1 Mev per nucleon are measured as a function of absorber thickness, and the thickness necessary to stop the beam completely is determined. The results are analyzed by a method based on a comparison with the proton range-energy relation.[6] Systematic changes in the shape of the range-energy curve are observed as the atomic number of the ion beam increases. The deviations are described quantitatively by assuming that the "effective charge" of the ion decreases in accordance with a simple empirical formula as the ion velocity decreases. A single formula is successful for all beams studied and thus (presumably) can be used as a basis for the prediction of range-energy curves in aluminum. The equilibrium distribution of charge states also can be obtained from the data, and preliminary results for the case of O^{16} ions in aluminum are discussed in relation to the range results.

B. Experimental Method

The heavy-ion accelerator produces a beam of ions of "energy" $\mathcal{E}_m^0 \approx 10$ Mev/amu.[22] To insure that $\mathcal{E}_m^0$ is constant and sharply defined, the beam is passed through an analyzing magnet of high resolution before being brought to a focus in the experimental area. In this experiment a known thickness X of aluminum absorber foil is placed in the path of the incident beam, reducing its mean energy from $\mathcal{E}_m^0$ to $\mathcal{E}_m$. A magnetic spectrograph is used to analyze the beam emerging from the foil and determine $\mathcal{E}_m$. The variation of $\mathcal{E}_m$ with X is found by making measurements with foils of many different thicknesses. Since X is equal to the difference between the range $R^0(\mathcal{E}_m^0)$ of the incident ions and the range $R(\mathcal{E}_m)$ of the emergent ions, the experimental results may be regarded as measurements of the range difference, $R^0(\mathcal{E}_m^0) - R(\mathcal{E}_m)$, as a function of $\mathcal{E}_m$.

Figure 1 is an idealized sketch of the spectrograph used for the energy measurement. The ion beam, sharply collimated in a field free region, abruptly enters a uniform magnetic field of strength B_0. The incident path is perpendicular to the edge of the field and to the lines of force. In the field the ions follow circular orbits of radius $r = kp/(B_0 Z)$, where p is the momentum of the ion, Z is its charge, and k is a constant determined by the system of units used. If a strip of photographic film is placed as shown on a circle of diameter a (the

[5] H. Bichsel, R. F. Mozley, and W. A. Aron, Phys. Rev. **105**, 1788 (1957).
[6] H. Bichsel, Phys. Rev. **112**, 1089 (1958).
[7] N. Bohr, Phys. Rev. **58**, 654 (1940); **59**, 270 (1941).
[8] J. Knipp and E. Teller, Phys. Rev. **59**, 659 (1941); J. H. M. Brunings, J. K. Knipp, and E. Teller, Phys. Rev. **60**, 657 (1941).
[9] N. Bohr, Kgl. Danske Videnskab. Selskab, Mat.-fys. Medd. **18**, No. 8 (1948); N. Bohr and J. Lindhard, Kgl. Danske Videnskab. Selskab, Mat-fys. Medd. **28**, No. 7 (1954).
[10] G. I. Bell, Phys. Rev. **90**, 548 (1953).
[11] R. L. Gluckstern, Phys. Rev. **98**, 1817 (1955).
[12] I. S. Dmitriev, J. Exptl. Theoret. Phys. (U.S.S.R.) **32**, 570 (1957) [translation: Soviet Phys.-JETP **5**, 473 (1957)].
[13] A. Papineau, Compt. rend. **242**, 2933 (1956).
[14] D. L. Livesey, Can. J. Phys. **34**, 203 (1956).
[15] W. H. Barkas, Phys. Rev. **89**, 1019 (1953).
[16] H. L. Reynolds, D. W. Scott, and A. Zucker, Phys. Rev. **95**, 671 (1954); H. L. Reynolds and A. Zucker, Phys. Rev. **96**, 393 (1954); W. H. Webb, H. L. Reynolds, and A. Zucker, Phys. Rev. **102**, 749 (1956).
[17] W. E. Burcham, Proc. Phys. Soc. (London) **70**, 309 (1957).
[18] Yu. Ts. Oganesyan, J. Exptl. Theoret. Phys. (U.S.S.R.) **36**, 936 (1959) [translation: Soviet Phys.-JETP **9**, 661 (1959)].
[19] H. H. Heckman, B. L. Perkins, W. G. Simon, F. M. Smith, and W. H. Barkas, Phys. Rev. **117**, 544 (1960).
[20] Independent investigations of heavy ion ranges recently have been completed by P. G. Roll and F. E. Steigert, Nuclear Phys. **17**, 54 (1960), and by E. L. Hubbard and J. Walton (private communication).
[21] In addition to the results reported here, energy loss measurements for heavy ions in Mylar and polyethylene are presented in a companion paper, P. E. Schambra, A. M. Rauth, and L. C. Northcliffe, following paper [Phys. Rev. **120**, 1758 (1960)].
[22] All of the various ion beams emerge from the Yale heavy-ion accelerator with the same velocity. Furthermore, the energy loss mechanisms are most comparable for different fast-moving ions when they have the same velocity. Since ions of different rest mass m and kinetic energy E have equal velocity when they have the same kinetic energy per unit mass, the quantity $\varepsilon_m \equiv E/m$ is taken to be more meaningful and convenient than the total kinetic energy E in this report.

"detector circle") which is tangent to the edge of the field at the point of incidence, then the measured deflection corresponding to an orbit of radius r will be $s=a\tan^{-1}(a/2r)$. It follows that the ion energy per unit mass is given by the relation

$$\mathcal{E}_m=\left(1-\frac{1}{4}\frac{\beta^2}{1-\beta^2}\cdots\right)\left(\frac{B_0}{K}\right)^2\left(\frac{Z}{m}\right)^2\cot^2\left(\frac{s}{a}\right), \quad (1)$$

where β is the ion velocity. The constant K is 11.342 in the spectrograph actually constructed (in which $a=254.05$ mm) when B_0 is expressed in kilogauss, Z in units of the electron charge, m in atomic mass units, and $\mathcal{E}_m$ in units of Mev per amu. The term involving β^2 is a relativistic correction which never exceeds 0.6% in this experiment.

For fixed values of B_0 and m, the ion energy is measured in terms of the quantity $Z\cot(s/a)$. When the nuclear charge of the ion is Z_0, then Z can assume integer values from 0 to Z_0 and a given value of $Z\cot(s/a)$ corresponds to a series of spectral lines at equally spaced values of $\tan(s/a)$. Usually two or three of the lines are observed. Their respective Z values are assigned so as to match the observed sequence of $\tan(s/a)$ values. The ion energy then can be calculated, each line providing an independent measurement of $\mathcal{E}_m$. Moreover, the equilibrium charge state distribution in the beam is shown by the relative intensity of the lines, and the energy distribution (i.e., straggling) is indicated by their broadness. Thus the spectrum contains a relatively complete description of the beam as it emerges from a given absorber foil, and this information is permanently recorded on photographic film. The data collection for a given beam and absorber material is complete when the spectra for absorber thicknesses of sufficient variety have been recorded. Since individual spectrum photographs usually require only short exposures it is practical to make similar measurements for a large number of different beams and absorbing materials.

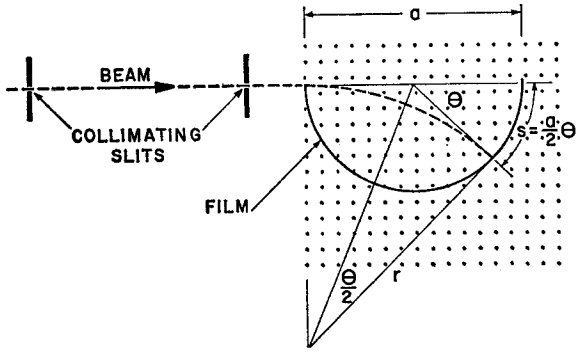

FIG. 1. Schematic diagram of the method used for the measurement of ion energy. The dotted region represents a uniform magnetic field of strength B_0 perpendicular to the page. The energy (per unit mass) of the ion is given in terms of its mass m, charge Z, and deflection s by Eq. (1).

There are few sources of systematic error in the energy measurement, and with reasonable care in the construction and alignment of the spectrograph all but one of these can be eliminated. The unavoidable complication arises because it is impossible in practice to terminate the uniform magnetic field with an edge of the ideal shape, a discontinuous drop to zero. The deviation from ideal edge shape causes a displacement of the ion orbit which must be taken into account. The complexity of this determination is reduced as much as possible by designing the spectrograph so that the ions encounter only one edge and approach it with normal incidence. Since there is negligible focusing with this arrangement, it is necessary to collimate the incident ions very sharply in order to obtain acceptable resolution. The resultant loss of intensity is not a serious disadvantage because the instrument is used to study direct beams. However, the fact that this equipment observes only a small portion of the degraded beam, excluding ions which have suffered appreciable deflection in the absorber, may be of significance in the interpretation of the results and in any comparison with results obtained by other methods.

II. EXPERIMENTAL DETAILS

A. Description of the Apparatus

A schematic plan view of the experimental apparatus is given in Fig. 2. The foil changer contains 19 selected thicknesses of aluminum foil (see Sec. II. E) mounted in a series of holes near the rims of two thin wheels. Since each foil from one wheel can be brought into the path of the beam together with any desired foil from the other wheel, a large variety of combined thicknesses can be obtained. After energy degradation in the foils the beam is monitored and collimated by a system of four slits. The first slit is $\frac{1}{8}$ in. in width and at ground potential while the second is $\frac{1}{32}$ in. in width and electrically isolated. Of the ions which pass through the first slit a large fraction are intercepted by the jaws of the second giving rise to the monitor signal. The last two slits are 0.005 in. in width and are separated by $\sim 12\frac{1}{2}$ in., thus serving to collimate the beam to a half-angle of 1.4 minutes of arc in the horizontal plane. In the region between the collimating slits a double-walled iron pipe shields the beam path from the fringing field of the spectrograph magnet and sharpens the transition from the field-free region to the region of uniform field B_0.

A small fraction of the incident beam survives the drastic collimation and enters the magnetic field. The field is monitored and measured by means of a proton resonance probe placed near the center of the magnet gap. Stabilization of the magnet current against short-term variations is achieved by regulation of the voltage on the magnet windings. Slow drifts in the magnetic field are revealed by the proton resonance signal, and

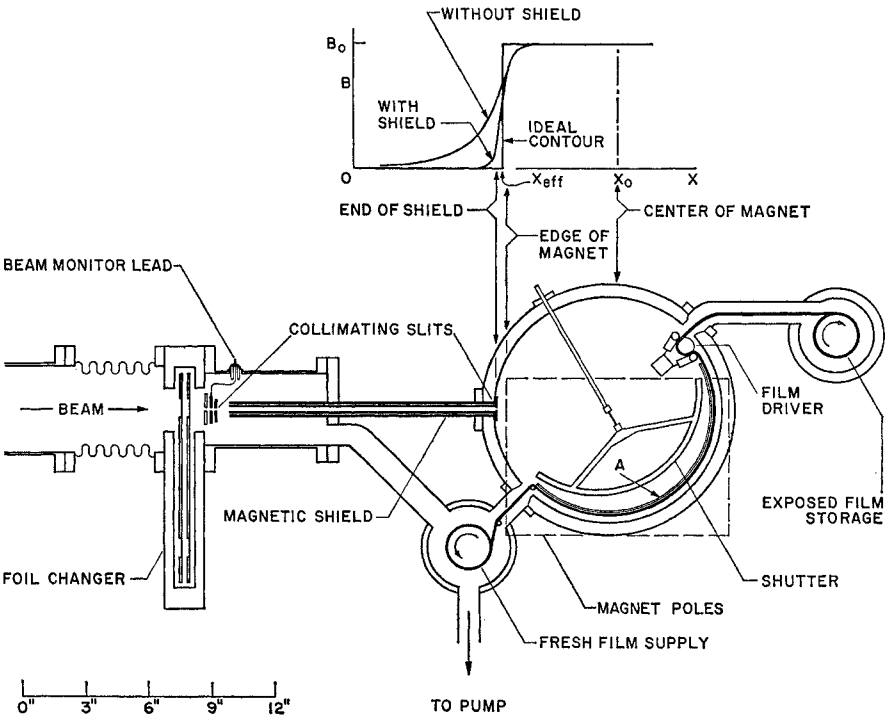

FIG. 2. Schematic plan view of the apparatus. The field contour plots in the upper part of the figure show the field variations along the incident beam axis with and without the magnetic shield, in comparison with the ideal contour assumed in Fig. 1. The detector (a strip of 16-mm motion picture film) is held in the proper position by the guide rail A, an enlarged section view of which is shown in Fig. 3. The shutter can be pushed against the guide rail to shield a region of the film reserved for particle detection while a flash of light is used to print a reference scale on the film.

correction for them is made by manual adjustment of the magnet current.

The vacuum chamber is made sufficiently rigid to withstand atmospheric pressure without appreciable deformation by the use of brass $\frac{5}{16}$ in. in thickness for its floor and ceiling. Since the magnet gap is only $1\frac{1}{2}$ in., this limits the interior height of the chamber to $\frac{7}{8}$ in. The chamber and collimating system are clamped to the magnet poles in a position precalculated to place the "effective edge" of the magnetic field at the first intersection of the beam path with the "detector circle" of the chamber, as assumed in Sec. IB. The detector circle is defined by an accurately machined guide rail of 10-in. diameter. A strip of commercial 16-mm motion picture film held against the guide rail under slight tension serves as the detector. The deflected ions strike the film with normal incidence, creating tiny spots which accumulate to form visible "spectral lines."

The necessary length of exposure varies from one second for ion beams near maximum energy to ~15 min for beams which are almost stopped by the absorber. Most exposures require one minute or less. Between exposures the film is advanced as in an ordinary camera, the exposed film moving to a storage reel while fresh film is drawn from a supply reel. During an exposure the supply reel is clamped and the film is drawn tight against the guide rail. More than one hundred exposures can be made before it is necessary to break the vacuum and splice in a new reel of film.

At the time of the exposure an accurate distance scale is printed on the film, providing a frame of reference for subsequent measurements. The scale is a row of very small printed spots, accurately spaced at 5-mm intervals along the strip of film. The mean spot spacing in a row is known within $\pm 0.05\%$ and the deviation of each individual spot from this mean is known within a few microns. Each spot is the radially

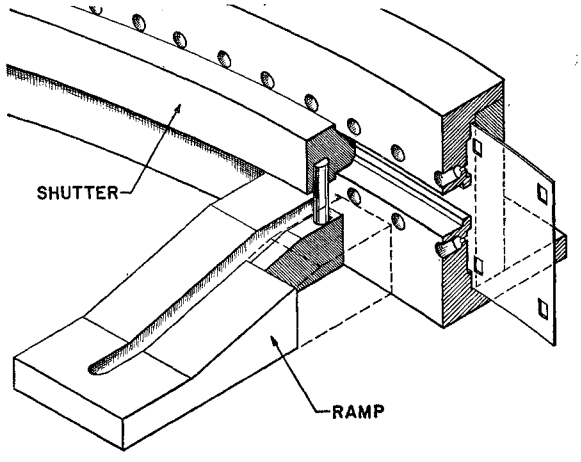

FIG. 3. Section view of the guide rail and shutter as seen from A of Fig. 2. The shutter (shown closed) protects the central band of film while a flash of light prints an image of the row of holes (the reference scale) onto the film. Each hole is constricted at its base to a diameter of ~$\frac{1}{4}$ mm. The movements of the shutter are guided by four slotted ramps, only one of which is shown. When the shutter is retracted it slides down the ramps and rests on the chamber floor, allowing the ions to pass through the slot in the guide rail and be recorded on the film.

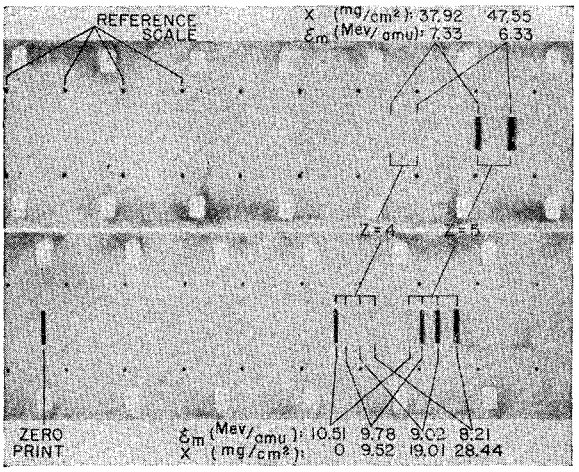

FIG. 4. Two representative film strips obtained with the apparatus of Fig. 2, showing the reference scale, several spectral lines (by multiple exposure), and a beam print made with the magnet current turned off (i.e., the "zero" of the reference scale). The incident beam is $B^{11}(4+)$, and the initial ion energy (per unit mass) is fixed at $\mathcal{E}_m{}^0=10.51$ Mev/amu. The spectra correspond to six different thicknesses X of absorber placed in the path of the beam. The positions of the spectral lines for $Z=4$ and $Z=5$ are indicated for each absorber thickness, along with the emergent ion energy per unit mass ($\mathcal{E}_m \equiv E/m$) as determined from the line position. The faint line for $Z=5$ with no absorber is explained by charge exchange occurring in the residual gas of the vacuum system, between the magnetic analyzer and the spectrograph. The almost complete conversion to $Z=5$ is expected when absorbers are used. At each energy the equilibrium charge distribution of the ions can be inferred from the relative line intensity, and the energy straggling from the linewidth.

projected image of a very fine hole in the guide rail (see Fig. 3), printed by light from a tungsten filament source at the center of the chamber.

In Fig. 4 two typical sections of film are reproduced. The "zero print" fixes the absolute position of the reference scale. It is obtained by turning the magnet current off and allowing the "undeflected" beam to strike the film (a small deflection caused by the residual field is easily calculated). The use of multiple exposures is a time-saving measure. The broadening of the spectral lines with decreasing energy is largely a result of energy straggling in the absorber foils.

B. Field Deviations

As shown by the contour plot in Fig. 2, the actual field contour is only an approximation to the ideal assumed in Sec. IB. Consequently, the orbit is distorted from its ideal shape. Within the uniform field the net result is a horizontal displacement of the orbit by an amount Δx along the incident beam axis and an amount Δy normal to the axis, along with a small rotation $\delta y/D$ about a vertical axis through the first collimating slit (D is the distance between the collimating slits). The quantities Δx, Δy, and δy can be calculated if the actual field contours are known, and it is then a simple problem in geometry to find the correction for the spectral line position.

TABLE I. Orbit correction parameters obtained by integration of measured field contours. The values for Δx, the deviation from ideal placement of the detector circle, are subject to a uniform uncertainty of ~0.0025 in. largely arising from the uncertainty in the location of the center of the magnet. The quantities $r_0\Delta y$ and $r_0\delta y$, which characterize the lateral displacement and the rotation of the orbit, respectively,[a] are assigned an uncertainty of ±20% because of the complexity of their determination. Independent determinations of the parameters gave values falling well within the assigned uncertainties. The fractional correction to the ion energy ($\delta\mathcal{E}_m/\mathcal{E}_m$) is found to be approximately constant. The magnitude of this correction is given for the spectrograph fields actually used, along with its uncertainty as derived from the uncertainty of the orbit correction parameters.

	B_0(kilogauss)				
	1.4	4.0	10	12	14.5
Δx (in.)	−0.001	−0.001	−0.005	−0.008	0.0088
$r_0\Delta y$ (in.²)	0.051	0.051	0.058	0.084	0.162
$r_0\delta y$ (in.²)	0.0004	0.0004	0.002	0.007	0.038
$\delta\mathcal{E}_m/\mathcal{E}_m$	0.23±0.11%	0.23±0.11%	0.40±0.11%		

[a] The quantity r_0 is the radius of the ion orbit within a uniform field of strength B_0.

The field shape was investigated using a Rawson rotating coil fluxmeter having a search coil only 3 mm in diameter so that the rapid field variations at the edge of the magnet could be determined with reasonable accuracy.[23] The measured contours were analyzed by two independent methods (one graphical, one utilizing formulas fitted to the contours) and the results are summarized in Table I.

The nonuniformity of the central field (including the end of the trajectory at the back edge of the magnet) causes a negligible distortion of the orbit at the fields used. However, a central field nonuniformity also can introduce an error in B_0, because of the difference in location of the orbit and the proton resonance probe. This error was negligible at 1.4 and 4.0 kilogauss and not greater than ~0.05% at 10 kilogauss. No correction was applied for it but an additional uncertainty of 0.1% is assigned to $\mathcal{E}_m$ values obtained with $B_0=10$ kilogauss.

C. Geometric Factors

The guide rail and the chamber containing it were lathe-turned to fit together as an accurately circular and concentric assembly. The detector circle diameter a was found to be 10.002±0.001 in. by micrometer measurement of the guide rail; both the uncertainty in a and the corresponding uncertainty in K are negligible. The reference scale holes were drilled through the guide rail on a milling machine fitted with an accurately divided rotary table. Although the systematic error in mean hole spacing is negligible, the random fluctuation of holes about the mean spacing leads to an uncertainty of ±0.05% in the absoluteness of the scale. Alignment of the center of the detector circle on the axis of the collimating slits was achieved within 0.005

[23] The measurements were made in a rectangular coordinate system fixed with respect to the magnet. The placement of the magnet in this coordinate system was determined within ±0.0025 in. by finding the center of magnetic symmetry with the beam shield temporarily removed.

in. using a beam of light projected through the slits. The error arising from a misalignment of 0.005 in. would be negligible.

D. Film Measurements

The spectral line for a monoenergetic incident beam has a minimum width of $\sim\frac{1}{4}$ mm, and the width is even greater when the beam is not monoenergetic. Therefore, the films were scanned with an optical densitometer and the line positions determined from a chart recording of the output, essentially a magnified plot of optical density vs distance along the film strip. Razor marks made in the film surface provided sharp secondary reference peaks on the densitometer plots. Their placement relative to the primary scale (the row of printed spots) was determined with a comparator. The placement of symmetrical lines relative to the primary reference scale easily could be determined within ± 0.012 mm under good conditions. The placement of the zero print relative to the reference scale was more carefully determined, and known within ± 0.005 mm. The over-all uncertainty in s (± 0.017 mm) corresponds to an uncertainty of $\sim 0.1\%$ in $\mathcal{E}_m$ with a field of 10 kgauss.

The variation of optical density with the number of ions detected per unit area of the film was found empirically. Thus the distribution of ion deflections could be determined from the densitometer plots and appropriately integrated to give the charge state distributions. When the spectral line is very broad, the distribution of ion deflections differs in shape from the distribution of ion energies. In such cases the densitometer plot was appropriately transformed into an energy distribution to get the mean ion energy. When instrumental contributions are subtracted from the peak width, the remainder is a parameter describing the straggling in energy.

E. Absorber Foils

The absorber foils were cut from sheets of high-purity commercial aluminum using a precision punch of $1\frac{1}{4}$-in. diameter. Absorbers of differing thickness were obtained by stacking foils of an appropriate unit thickness. For one wheel of the foil changer (the A wheel) the unit thickness was 9.50 mg/cm^2 (actually achieved by combining two thinner foils) while for the second (the B wheel) the unit thickness was 1.15 mg/cm^2. The B wheel contained nine stacks of foil ranging in thickness from 1.15 to 10.31 mg/cm^2 in approximately equal steps, while the A wheel contained 10 stacks ranging in thickness from 9.52 to 95.11 mg/cm^2 in approximately equal steps. Before the experimental runs began, a preliminary determination of the foil stack thicknesses was made by weighing each stack on a semimicrobalance and measuring the diameter of typical foils with a comparator (155 foils were used in the foil changer and the careful measurement of every area was not considered to be practical). At the conclusion of the runs a more precise set of measurements was made on the thick (A) foils to insure against systematic errors. For this second set of measurements a smaller section, 22 mm square, was cut from the center of each circular foil using a template and a razor blade. Each stack of foils was weighed on an accurate microbalance, taking the buoyancy of air into account. It was determined that solvent cleaning of the foils caused no significant change in their weight. Ten representative foil squares then were measured on a comparator and a "best" value for the area of a square was inferred from the measurements. Nine of the 10 squares had areas within 0.1% of the "best" area, the tenth foil differing by 0.2%. This "best" area was assumed for the foils not measured on the comparator. Since the error in foil area of an occasional deviant would be diluted by the presence of many foils of more nearly correct area, it is reasonable to assume that the over-all uncertainty in foil area is $\sim 0.1\%$ for the A foils. The weighing uncertainty for the foil squares was ± 0.03 mg, corresponding to a negligible uncertainty of ± 0.006 mg/cm^2 in the foil thickness. Thus the uncertainty of the A foil thicknesses is taken to be $\pm 0.1\%$. The accuracy requirements on the measurement of B foil thicknesses are less stringent because these foils serve only as interpolations between the larger A foil steps. Errors in their determination are revealed by periodicity in the experimental range-energy curve and these errors are not cumulative. Therefore, the preliminary determinations of the B foil thicknesses were judged to be sufficiently accurate. The uncertainties in B foil thickness were estimated to be ± 0.04 mg/cm^2.

Because the largest absorber thickness obtainable with the foil changer (105.42 mg/cm^2) was insufficient to stop the He^4 beam, provision was made for the insertion of a special "thick absorber" when needed. The "thick absorber" was independent of the foil changer and could be used in conjunction with it to extend the range of available absorber thicknesses. It also was constructed by stacking several thinner foils, and its over-all thickness was measured to be 122.45 ± 0.12 mg/cm^2.

No estimate of errors caused by nonuniformity of foil thickness has been included in the above discussion and such errors easily could be as large as the uncertainties in the measurement of the average foil thickness. However, the large number of foils in each absorber and the large number of absorber changes during a run should tend to diminish the effect of these errors.

F. Procedure

During the study of each ion beam the current in the magnetic analyzer was held constant. The analyzer slits were set to give a nominal resolution of $\pm 0.2\%$ for the energy of incident He^4, N^{14}, and O^{16} beams, and $\pm 0.1\%$ for incident beams of B^{10}, B^{11}, C^{12}, F^{19}, Ne^{20}. In

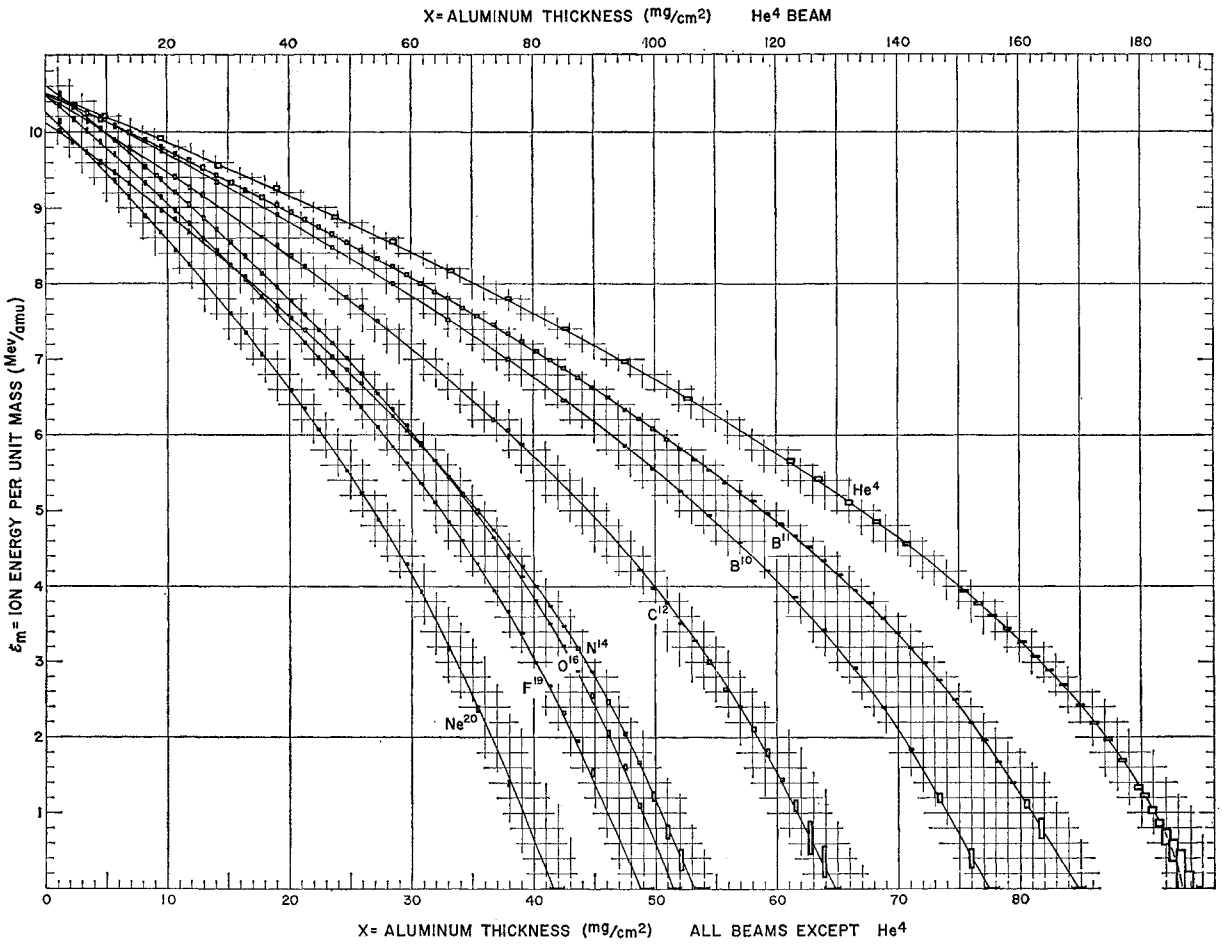

FIG. 5. Graphical display of the experimental results, showing the emergent ion energy per unit mass ($\mathcal{E}_m$) for various heavy ions as a function of the thickness (X) of aluminum absorber through which they have passed. Since X may also be interpreted as the range difference $R^0(\mathcal{E}_m^0)-R(\mathcal{E}_m)$, the curves may be regarded as range-energy relations. The experimental points are plotted as rectangles to indicate two composite uncertainties (see text). For each beam a horizontal bar on the X axis indicates the pair of absorber thicknesses between which the transmitted beam current falls to zero. Note the difference in scale for the He^4 curve.

each case an upper limit for the range R^0 of the full energy beam was determined by increasing the absorber thickness X until the monitor signal disappeared. Then a large number of exposures were made for values of X distributed throughout the region $0\leq X\leq R^0$. The value of X was varied in a pattern designed to reveal time-dependent systematic errors and to suppress them in the average.

Three different values of spectrograph field normally were used. Most of the exposures were made with $B_0=10$ kgauss because the dispersion and resolution are highest with large fields. At low energies, however, the spectral lines are weakened, broadened, and more widely displaced, and the smaller value $B_0=4$ kgauss was more appropriate. At the lowest energies exposures with $B_0=1.4$ kgauss were valuable because of the faintness and extreme breadth of the lines. Usually the regions investigated with different fields were allowed to overlap. In the case of one beam, He^4, parallel sets of exposures over the full region of ion energy were obtained for the field values $B_0=1.4$, 4, 6, 8, 10, and $11\frac{1}{2}$ kilogauss to provide an extensive consistency check.

III. PRESENTATION OF THE RESULTS

The experimental results are presented in relatively raw form in Fig. 5. In general, several measurements of $\mathcal{E}_m$ were obtained for each absorber thickness, usually in agreement well within their respective accuracy assignments. Only the measurements of greatest inherent accuracy are plotted. The various experimental uncertainties in each measurement are combined to form two composite uncertainties, which are indicated for each point by showing it as a rectangle.

Experimental errors in the range-difference measurement arise not only from errors in the measurement of absorber thickness and emergent ion energy, but also from fluctuations of the incident ion energy

(within the resolution of the magnetic analyzer). However, the latter is equivalent to an additional uncertainty in absorber thickness. In the case of He^4 the added uncertainty is ± 0.60 mg/cm^2 but it is much smaller for all other beams, varying from ± 0.06 mg/cm^2 in the case of Ne^{20} to ± 0.18 mg/cm^2 in the case of N^{14}. These uncertainties are added to the actual uncertainties in foil thickness (Sec. II-E) to give the width of each rectangle. The height of each rectangle includes contributions arising from uncertainties in the measurement of Δx, Δy, δy, and B_0 (Sec. II. B), in the measurement of a and K, the geometric alignment, and the mean spot spacing of the reference scale (Sec. II. C), and in the determination of spectral line position relative to the reference scale (Sec. II. D). Of these, only the last represents an error which fluctuates from point to point in a random fashion. The others are estimated limits for systematic errors. The linear sum of these systmatic error estimates amounts to a fractional error $\delta\mathcal{E}_m/\mathcal{E}_m$ of $\pm 0.35\%$ with a spectrograph field of 10 kilogauss and less for smaller fields. The uncertainty in spectral line position, on the other hand, corresponds to an energy uncertainty which is only 0.10% for ion energies above 5 Mev/amu but increases as the spectral line broadens with decreasing ion energy and becomes very large at the lowest energies where the spectral lines overlap. The height of each rectangle shows the square root of the quadratic sum of these two uncertainties in $\mathcal{E}_m$.

Where the curves of Fig. 5 intersect the X axis a horizontal bar is drawn for each beam to indicate the pair of X values between which the monitor signal vanishes. This serves roughly to indicate the full range $R^0(\mathcal{E}_m{}^0)$ of the incident beam. If $R^0(\mathcal{E}_m{}^0)$ were known accurately for each beam, range-energy curves could be displayed directly. This is not done because the accuracy of the measured X values would be obscured by the large uncertainty in $R^0(\mathcal{E}_m{}^0)$ (except in the case of He^4, discussed in Sec. VA).

IV. METHOD OF ANALYSIS

The fluctuations of the experimental data and the experimental uncertainties are too small in general to be studied effectively in terms of a plot such as Fig. 5. In the analysis to be described, the heavy-ion data are compared with a formula for the range-energy relation of protons in aluminum,[6] using the elementary theory of the energy loss process.[24] According to this theory the "stopping power" $-d\mathcal{E}_m/dX$ for a heavy ion of charge Z, mass m, and velocity v is given by the relation $-d\mathcal{E}_m/dX=(Z^2/m)f(v)$, where $f(v)$ is a function of the stopping material as well as the ion velocity but is independent of m. If it is assumed that $f(v)$ also is independent of Z, then for a given absorbing material $f(v)$ is a function of the ion velocity only. In general, because of electron capture by the ion, the charge Z will not be the nuclear charge Z_0 of the ion but some smaller "effective charge" $Z_{\text{eff}}=\gamma Z_0$, where $0\leq\gamma\leq 1$. The value of the effective-charge parameter γ will vary with v and depend on Z_0 but presumably will be independent of m. It is convenient to define a "universal" measure of absorber thickness $X_m\equiv XZ_0^2/m$ to replace the conventional thickness X. The stopping-power formula then takes on the simple "universal" form

$$-d\mathcal{E}_m/dX_m=\gamma^2 f(v). \tag{2}$$

Since ions which have the same value of $\mathcal{E}_m$ are moving with the same velocity regardless of their mass, Eq. (2) shows that the value of $d\mathcal{E}_m/dX_m$ is the same for all ions of the same energy $\mathcal{E}_m$ (neglecting the dependence of γ on Z_0), which means that the graph of $\mathcal{E}_m$ vs X_m is the same for all ions. The degree to which this is true is shown in Fig. 6. Since $f(v)$ is assumed to be independent of ion identity the differences between the curves are attributed to differences in γ. If γ is dependent on Z_0 (and v) but not on m, as has been assumed, then the curve is the same for all ions of the same chemical element. Consistent with this assumption, the two separate solid curves through the points for B^{10} and B^{11} in Fig. 5 actually are drawn so as to be equivalent to the single curve given for boron ions in Fig. 6. The good agreement between the solid curves and the experimental data lends support to this assumption, enhancing the significance of the curves of Fig. 6. From these "universal" curves it is possible to infer range-difference vs energy curves for beams of all isotopes in the range $5\leq Z_0\leq 10$. Moreover, it is apparent that "universal" curves for Li and Be ions can be estimated with very little uncertainty, by virtue of the

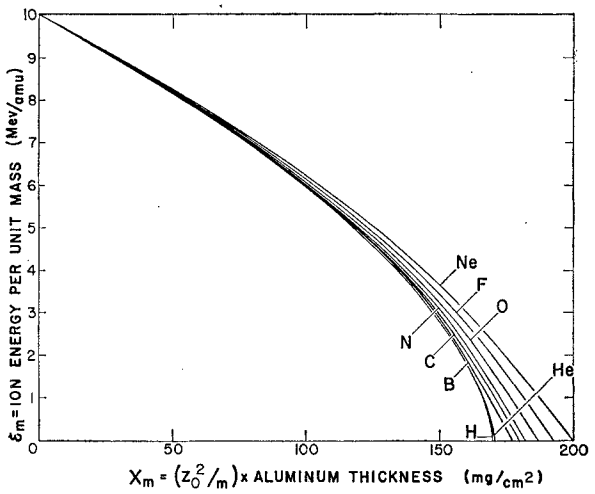

FIG. 6. The curves of Fig. 5 redrawn in terms of the "universalized" measure of absorber thickness, $X_m\equiv(Z_0^2/m)X$. The curves also are displaced horizontally so as to correspond to the same initial ion energy, $\mathcal{E}_m{}^0=10$ Mev/amu. The curve for boron is equivalent to the two curves for B^{10} and B^{11} in Fig. 5. The curve for protons is based on the experimental results of Bichsel (reference 6) as embodied in Eq. (4).

[24] See, e.g., H. A. Bethe and J. Ashkin, *Experimental Nuclear Physics*, edited by E. Segrè (John Wiley & Sons, New York, 1953), Vol. I, part II.

near coincidence of the "universal" curves for He and B ions. Thus range-difference predictions can be made for all isotopes up to and including those of neon.

Since $\gamma=1$ for protons having energy $\mathcal{E}_1$ greater than $\frac{1}{2}$ Mev/amu, it is apparent from Eq. (2) that a measurement of the proton range-energy relation in any material may be interpreted as a measurement of $f(v)$ for that material. Thus Eq. (2) may be rewritten in the form

$$d\mathcal{E}_m/dX_m=\gamma^2 d\mathcal{E}_1/dX_1, \tag{3}$$

where the subscript 1 is used to identify quantities $\mathcal{E}_m$, X_m, etc., when they apply to the proton. (The subscript is used only as an identification since the proton is compared with ions of the same velocity and the quantities $\mathcal{E}_m$ and $\mathcal{E}_1$ always are numerically equal.) In the recent experiments of Bichsel *et al.*[5,6] proton ranges were measured in aluminum with an accuracy of 0.2% for the energy region $1.12\leq\mathcal{E}_1\leq 18$ Mev/amu. Bichsel gives formulas[6] for the proton range which fit his experimental results within that accuracy. When expressed in terms of $\mathcal{E}_m$ and $R_m\equiv RZ_0^2/m$, the formulas become

$$R_1=\frac{R(\text{mg/cm}^2)}{1.0076(\text{amu})}=\begin{cases}3.854\mathcal{E}_1^{1.5874}; & 1.12\leq\mathcal{E}_1\leq 2.657 \text{ Mev/amu}\\ \dfrac{2.8585\mathcal{E}_1^2}{0.6833+\log_{10}\mathcal{E}_1}; & 2.657\leq\mathcal{E}_1\leq 18 \text{ Mev/amu},\end{cases} \tag{4}$$

where $\mathcal{E}_m=\mathcal{E}_1=(E/1.0076)$ Mev/amu. Formulas for $d\mathcal{E}_1/dX_1(=-d\mathcal{E}_1/dR_1)$ are obtained easily by differentiation of Eq. (4).

Using Eq. (4) the proton range-difference

$$R_1^0(\mathcal{E}_1^0)-R_1(\mathcal{E}_1)=X_1(\mathcal{E}_1^0,\mathcal{E}_1)$$

can be calculated as a function of $\mathcal{E}_1$. This curve, calculated for $\mathcal{E}_1^0=10$ Mev/amu, is plotted in Fig. 6 along with the comparable curves for heavier ions. It is noted that the range-difference curve for He^4 ions coincides with the curve for protons, as predicted, in the energy region above 1 Mev/amu where the value of γ^2 for the alpha particle is known to be unity.[25] In most cases, however, the observed heavy-ion range-difference $X_m(\mathcal{E}_m^0,\mathcal{E}_m)$ is larger than the calculated proton range-difference $X_1(\mathcal{E}_1^0,\mathcal{E}_1)$ by an amount Δ_m, for the comparable energies $\mathcal{E}_1^0=\mathcal{E}_m^0$ and $\mathcal{E}_1=\mathcal{E}_m$. There is much to be gained if the analysis is carried out in terms of the quantity Δ_m, which may be defined explicitly by the relation

$$\Delta_m\equiv[X_m(\mathcal{E}_m^0,\mathcal{E}_m)-X_1(\mathcal{E}_1^0,\mathcal{E}_1)]. \tag{5}$$

The gross dependence of X_m on $\mathcal{E}_m$ is removed mathematically while the experimental deviations are retained in the residual and are greatly exaggerated. These deviations include random and systematic errors as well as the real physical deviation. The residuals are similar in magnitude and energy dependence for the various ion beams and can be compared in detail. Thus, systematic errors are located and identified more easily, and the "true" form of the deviation (i.e., that associated with the variation of γ^2) can be estimated with the maximum accuracy allowed by the experimental uncertainties. Furthermore, the stopping power $-d\mathcal{E}/dX$ and the effective charge parameter γ^2 can be determined easily and with the greatest obtainable accuracy from the variation of Δ_m with energy. The stopping power is given in terms of $d\Delta_m/d\mathcal{E}_m$ by the expression

$$\frac{d\mathcal{E}_m}{dX_m}=\left[\frac{dX_1}{d\mathcal{E}_1}+\frac{d\Delta_m}{d\mathcal{E}_m}\right]^{-1}, \tag{6}$$

and γ^2 is given by the expression

$$\gamma^2=\frac{d\mathcal{E}_m}{dX_m}\frac{dX_1}{d\mathcal{E}_1}=\left[1+\frac{d\Delta_m}{d\mathcal{E}_m}\frac{d\mathcal{E}_1}{dX_1}\right]^{-1}. \tag{7}$$

Alternatively, if the energy dependence of γ^2 is known or can be estimated, the value of Δ_m (and thus the range difference) can be calculated using Eq. (7) in its integrated form,

$$\Delta_m=\int_{\mathcal{E}_1^0}^{\mathcal{E}_1}\left[\frac{1}{\gamma^2}-1\right]\frac{dX_1}{d\mathcal{E}_1}d\mathcal{E}_1. \tag{8}$$

Actually, the data are plotted in terms of the quantity $(m/Z_0^2)\Delta_m\equiv\Delta$ rather than in terms of Δ_m, since the scaling factor m/Z_0^2 decreases the difference between the residuals for the various ion beams and makes their comparison easier. Moreover, the quantity Δ has a simple practical interpretation, as can be seen by rewriting Eq. (5) to give the heavy-ion range difference in conventional thickness units,

$$X(\mathcal{E}_m^0,\mathcal{E}_m)=\frac{m}{Z_0^2}\{R_1^0(\mathcal{E}_1^0)-R_1(\mathcal{E}_1)\}+\Delta(\mathcal{E}_m^0,\mathcal{E}_m). \tag{9}$$

Since the term containing brackets can be calculated using Eq. (4) (with $\mathcal{E}_1^0=\mathcal{E}_m^0$ and $\mathcal{E}_1=\mathcal{E}_m$) and may be regarded as the *predicted* heavy-ion range difference, Δ is the *excess* (in conventional thickness units) of the observed range difference over that predicted from the proton range difference. The use of Δ rather than Δ_m is not without disadvantage, however, since the value of Δ for a given Z_0 varies with m while the value of Δ_m does not. Although the data are most conveniently

[25] Actually, there are small deviations from $\gamma^2=1$ for alpha particles with energies above $\mathcal{E}_m=1$ Mev/amu, although the deviations are too small to give rise to observable effects in this experiment. [The value of γ^2 can be deduced, by means of Eq. (11), from the alpha-particle charge measurements of G. H. Henderson, Proc. Roy. Soc. (London) **A109**, 157 (1925); G. H. Briggs, Proc. Roy. Soc. (London) **A114**, 341 (1927); and others.]

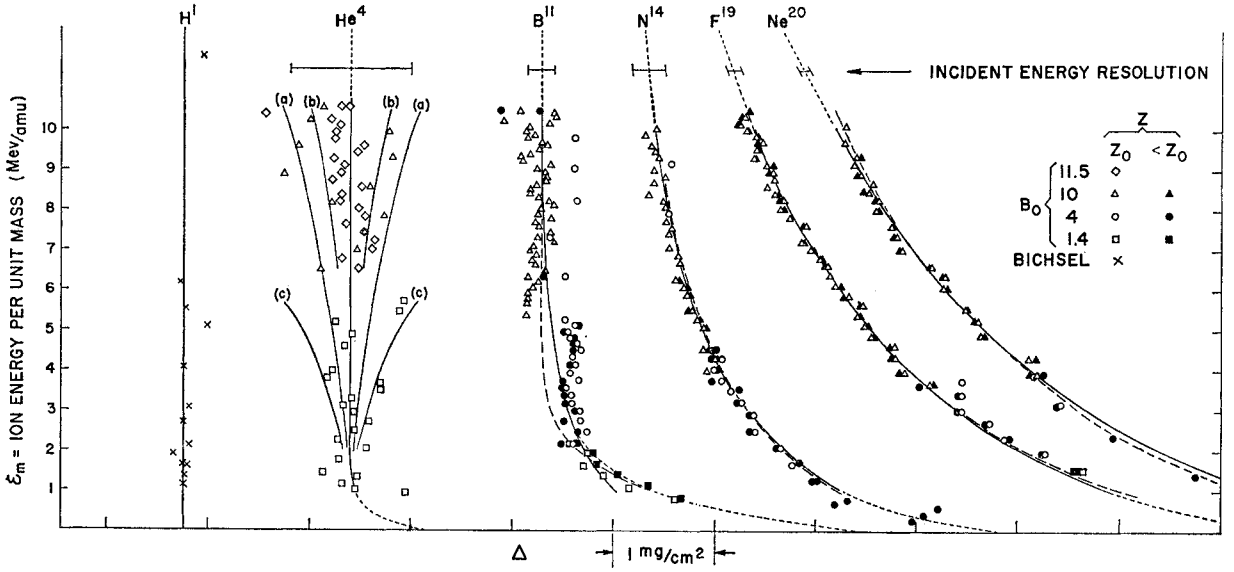

FIG. 7. Display of representative data by means of Δ plots. The quantity Δ is the difference between an experimental X value (at a given energy $\mathcal{E}_m$) and the value of X predicted from the proton range-energy curve [Eq. (4)], assuming that $\gamma=1$. The fluctuations of Δ caused by incident-beam energy variations within the resolution of the magnetic analyzer are independent of $\mathcal{E}_m$ and are shown above each plot. The deviation from vertical of either curve (a) on the Δ plot for He^4 shows the distortion that would accompany a systematic error of 0.2% in the measurement of $\mathcal{E}_m$, while curves (b) and (c) show the distortion caused by a systematic error of 0.020 mm in the measurement of spectral line position, at spectrograph fields of 10.0 and 1.4 kilogauss, respectively. For other beams the magnitude of such distortions diminish in proportion with the value of m/Z_0^2. On each plot, the first estimate for the "true" shape is shown by a dashed line, the shape implied by Eq. (10) is shown by a solid line, and the final choice for the "true" shape is indicated (when it differs from the solid line) by a dotted line. The Δ plot shown for H ions represents a comparison of the experimental data obtained by Bichsel with his formula [Eq. (4)].

plotted in terms of Δ they are more easily analyzed, summarized, and generalized in terms of Δ_m.

Some of the experimental results are presented in Fig. 7 in the form of "Δ plots."[26] The data were converted to this form using Eq. (9); the constant $\mathcal{E}_1^0$ was chosen arbitrarily and the value of Δ was calculated for each experimental point $(X,\mathcal{E}_m)$ using the measured value of $\mathcal{E}_m$ in place of $\mathcal{E}_1$. In order to display all of the results on one graph and at the same time separate the results for different beams, an arbitrary constant (different for each beam) was added to the calculated values of Δ.

For comparison the experimental points obtained by Bichsel[6] for a proton beam also are displayed by means of a Δ plot in Fig. 7, showing the extent of agreement between Bichsel's formula [Eq. (4)] and the data which served as a basis for its construction. It should be noted that the two formulas of Eq. (4) do not agree exactly at the overlap energy, $\mathcal{E}_m=2.657$ Mev/amu, and that their derivatives also are different at that energy. The discrepancy in Δ is $0.04m/Z_0^2$ mg/cm² and the discrepancy in $d\Delta/d\mathcal{E}_m$ is $0.173m/Z_0^2$ mg/cm² per Mev/amu. While these discrepancies are large enough to be visible on the Δ plots, they are smaller than the experimental uncertainties.

V. DISCUSSION

A. Alpha Particles

Because the effects of energy straggling are largest with He^4 ions, the broadening of a spectral line with decreasing energy is more pronounced than with heavier ions. However, a negligible fraction of He^4 ions have $Z=1$ at the energies encountered and only one spectral line is observed in each exposure. The peak on the densitometer plot is broad and distorted but not confused by the overlapping of neighboring spectral lines and thus can be transformed into an energy distribution (Sec. IID). For heavier ions this procedure seldom is necessary; whenever the line is so broad that its distortion would give rise to a significant error, the uncertainty caused by overlapping of lines is even greater.

Only a representative fraction of the data obtained with the He^4 beam are plotted in Fig. 7. Within their assigned uncertainties all points (including those not plotted) are consistent with the assumption that the "true" plot is the straight vertical line shown. There is

[26] The data for B^{10}, C^{12}, and O^{16} are omitted in the interest of simplicity. The plot for O^{16} ions is similar in appearance to the plots for N^{14} and F^{19} ions. The B^{10} data are much less complete than the B^{11} data but the Δ plots are not discernably different in shape. A variety of circumstances conspired to make the C^{12} data the poorest of the experiment. Many of the exposures were discarded and large uncertainties were assigned to others. Nevertheless, the C^{12} results are internally consistent within ±0.5 mg/cm² and the Δ plot is in harmony with those for other beams. Because of the usefulness of the results and their consistency with the better data, they are included despite their greater inherent uncertainty.

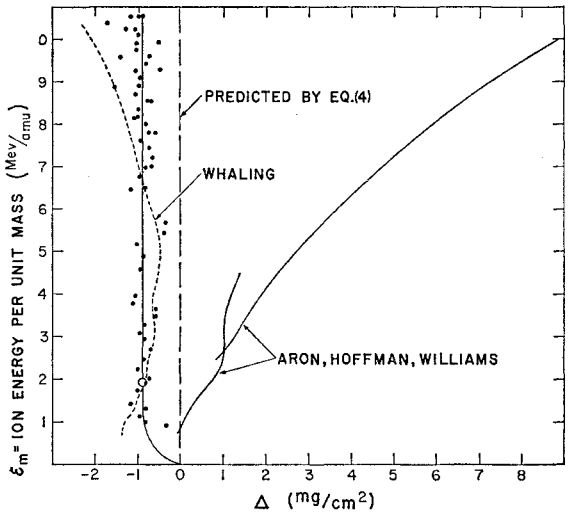

FIG. 8. Comparison of the He^4 data with various predictions for the alpha-particle range in aluminum. The quantity Δ in this case is the deviation from the range predicted by Bichsel's formula [Eq. (4)] on the assumption that $\gamma=1$. The open circle represents the experimental alpha range measurement given by Rosenblum (reference 2). The data of this experiment are arbitrarily placed on the Δ scale to agree with Rosenblum's point. The predictions given in references 3 and 4 also are shown.

no significant indication of systematic deviation from this assumption. Two interpretations are possible. If the measurements reported in this paper are regarded as absolute measurements, the vertical straight line Δ plot confirms the assumption that $f(v)$ is the same for protons and alpha particles. Alternatively, if Bichsel's results and this simple application of the theory are correct, the observed Δ plot indicates that the absolute errors in energy measurement with this equipment are less than 0.2%.

The results of this experiment are least accurate near zero energy. However, if independent low-energy data of high precision are used in conjunction with these results, a range-energy curve of considerable accuracy can be obtained. Since deviations from a vertical straight line plot would not be expected above $\mathcal{E}_m=2$ Mev/amu, it is sufficient to determine the difference between the value of $\Delta(\mathcal{E}_m)$ at some energy $\mathcal{E}_m$ in the neighborhood of 2 Mev/amu and its value $\Delta(0)$ at zero energy. Using the results of Rosenblum,[2] the alpha-particle range at $\mathcal{E}_m=1.919$ Mev/amu (i.e., $E=7.680$ Mev) is 11.8 mg/cm², compared with the value 10.93 mg/cm² calculated by means of Eq. (4). Thus the difference, $\Delta(\mathcal{E}_m)-\Delta(0)$, is -0.87 mg/cm². In Fig. 8 the He^4 data are shown (as solid dots) on another Δ plot, the horizontal scale of which is chosen so that Δ becomes zero at zero energy. On this plot the values of Δ predicted by Eq. (4) lie on a straight vertical line through the origin, and the quantity $-\Delta(\mathcal{E}_m)$ is simply interpreted as the excess of a range value at energy $\mathcal{E}_m$ over that predicted by Eq. (4). The straight vertical line chosen as a best fit to the experimental data is placed so as to pass through Rosenblum's point, i.e., the experimental mean ranges are assumed to exceed those predicted using Eq. (7) by the constant amount 0.87 mg/cm² for energies above 2 Mev/amu. (The curvature of the Δ plot between 1 and 2 Mev/amu is drawn to conform with the variation of γ^2 as deduced from the measurements of Henderson and Briggs.[25]) For comparison, the range-energy data tabulated by Whaling[3] and the curves given Aron, Hoffman, and Williams[4] also are shown on this Δ plot, as deviations from the predictions of Eq. (4). The solid line through the experimental points (and the origin) is taken to be the best estimate of the "true" Δ plot for He^4 ions, and is used to obtain the solid curves given for He ions in Figs. 5 and 6.

An analysis of the densitometer plots to gain information on straggling is in progress. Preliminary measurements indicate that the distribution of ion energies is approximately Gaussian in the region $1\leq\mathcal{E}_m\leq3$ Mev/amu (with $\mathcal{E}_m{}^0=10.5$ Mev/amu) and that the half-width of the distribution (at the fractional height e^{-1}) is approximately 0.4 Mev/amu when $\mathcal{E}_m=1$ Mev/amu. An indication of the magnitude of this effect also is apparent in Fig. 5 in that the mean range of the full-energy He^4 beam falls short of the maximum absorber thickness for which the monitor signal was observed.

B. Heavier Ions

The Δ plots for ions heavier than He^4 show systematic deviations from a straight vertical line and the deviations increase with decreasing ion energy. This is consistent with the observation that two or more spectral lines usually are visible in exposures made with these beams, i.e., that γ^2 is less than unity. In some exposures two lines are sufficiently clear to yield accurate values of Δ and a pair of points is plotted in Fig. 7. In general the agreement between members of a pair is seen to be excellent. (In many cases the points coincide and one is displaced deliberately to show the duality of the measurement.) However, there is some systematic disagreement between measurements obtained with different spectrograph fields, and some evidence of irregularities associated with the use of particular absorber thicknesses. Discussion of these indications of error will be deferred until a preliminary analysis has been described.

The data for each beam first were examined in detail in order to arrive at the best possible estimate for the "true" shape of the Δ plot. These estimates are shown in Fig. 7 as dashed lines. The slope of each dashed line was measured at several values of $\mathcal{E}_m$ between 1 and 10 Mev/amu and, using Eq. (7), the value of γ^2 was calculated for each energy. The values of γ^2 are not plotted as functions of $\mathcal{E}_m$, however, because the probability of electron capture is determined by the ion velocity and the binding energy of the

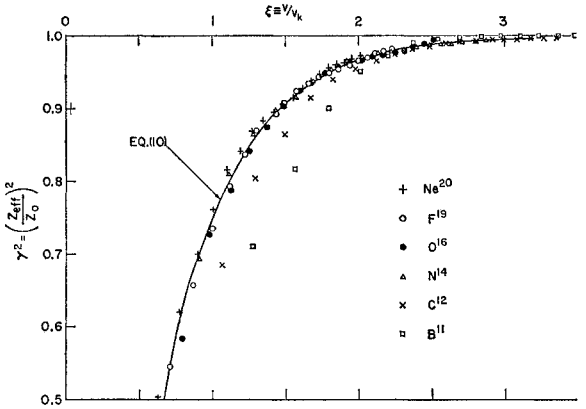

FIG. 9. Variation of the effective-charge parameter γ^2 with ion velocity. The parameter ξ is the velocity of the ion expressed in units of the Bohr orbital velocity v_k of its first k electron. The plotted points were obtained by measurement of the slopes of the dashed lines on the Δ plots of Fig. 7. The solid line is an empirical fit [Eq. (10)] to the points.

electron to the ion rather than the ion energy. According to a simple viewpoint[7,8] the significant parameter is the ratio of the ion velocity v to the orbital velocity of the electron being captured (or lost). Throughout most of the energy region the electron involved is the first k electron of the ion, and its orbital velocity v_k is given by the Bohr atomic model. In Fig. 9, the values of γ^2 are plotted as functions of the velocity ratio $\xi=v/v_k$. The most striking feature of this plot is the near coincidence of the results for Ne^{20}, F^{19}, O^{16}, and N^{14} ions. The solid line was obtained empirically and is given by the formula

$$\gamma^2=1-1.85e^{-2\xi}. \tag{10}$$

Although the values of γ^2 obtained with B^{11} and C^{12} beams deviate from this formula, it is not clear whether the deviations are real or merely arise from the relatively large uncertainty in the Δ plots for B^{11} and C^{12} ions. In any event, the simplicity of Eq. (10) and its apparent universality in the prediction of γ^2 for the heavier ions are of considerable practical importance, since Eq. (8) can be used to predict unmeasured ranges when γ^2 is known. The solid lines on the Δ plots of Fig. 7 were obtained by this method, i.e., by using Eq. (10) in Eq. (8) (the integral was evaluated graphically). Thus the solid lines represent the variations consistent with Eq. (10), and the extent of their agreement with the experimental data can be used to estimate the validity of Eq. (10). Moreover, the solid lines also aid in the detection of systematic errors since they represent the smooth behavior pattern of all of the data and a given value of γ^2 corresponds to a different pair of experimental parameters $\mathcal{E}_m$ and X for every beam.

In the case of Ne^{20}, F^{19}, O^{16}, and N^{14} there is little reason to doubt the validity of Eq. (10) since the solid lines follow the data very closely. The data for C^{12}, B^{10}, and B^{11}, on the other hand, contain irregularities which should be discussed. Although the Δ plots for C^{12} and B^{10} are not shown, the nature of the inconsistencies can be seen from the plot for B^{11}. For all three beams there are discontinuities in the Δ plot, associated with changes in the A absorber thickness. In the case of B^{11}, for example, these foil changes occurred at energies of $\mathcal{E}_m=6.4$, 5.25, 3.9, and 2.1 Mev/amu, and "steps" in the Δ plot accompany each change. Similar steps are observed for the same foil changes in the Δ plots for C^{12} and B^{10}. Since the magnitude of the steps generally is consistent with the uncertainty ($\pm 0.1\%$) of the A absorber thicknesses, most of the irregularities are attributed to small errors in the absorber thickness measurements. However, all of the inconsistency cannot be explained in this way. There remains a disagreement associated with a change in the spectrograph field, as is clearly shown by the plot for B^{11}. Similar discrepancies are observed in the data for B^{10} and C^{12} but it is significant that the discrepancy in the case of C^{12} is of the opposite sign. Moreover, the discrepancy appears to be independent of $\mathcal{E}_m$ when it occurs, and its magnitude varies from beam to beam in an irregular way. These observations are incompatible with the explanation of the discrepancy in terms of any known source of systematic error in the ion energy measurement, but all of them are consistent with the assumption of an incident beam energy shift within the resolution of the magnetic analyzer. Such shifts are easily explained by the "retuning" of the accelerator which always accompanied a change of spectrograph field. Thus, it is believed that the irregularities and discrepancies are not an indication of unknown systematic error. Moreover, the known experimental uncertainties are sufficient to explain the deviations of the data for B^{11} from the solid line curve predicted by Eq. (10). The data are fitted at least as well by the solid line curves as by the original dashed line curve, except at the lowest energies. (The same may be said in the case of B^{10} and C^{12}.) For these three cases the prediction of Eq. (10) is taken as the most reasonable estimate for the "true" shape of the Δ plot in the energy region $3\leq\mathcal{E}_m\leq 10$ Mev/amu. Below 3 Mev/amu the final curve is arbitrarily taken to deviate from the prediction (as illustrated by the dotted line on the Δ plot for B^{11}).

Range Differences

The solid line curves with the deviations and extrapolations indicated by dotted lines are taken as the final best estimates for the "true" shapes of the Δ plots. The values of $\Delta_m\equiv(Z_0^2/m)\Delta$ corresponding to these Δ plots are given in Table II. For convenience, the value $\Delta_m=0$ is assigned to ions of incident energy $\mathcal{E}_m^0=10$ Mev/amu. The value of $X_m(10,\mathcal{E}_m)$ can be obtained readily for each ion beam by using the tabulated quantities in Eq. (5). The curves for X_m given in Fig. 6 are plots of these values, and the solid line curves shown in Fig. 5 also are derived from these values. The range difference for any isotope (e.g., N^{12},

TABLE II. Final presentation of the experimental range-difference results for heavy ions in aluminum, in terms of the quantity $\Delta_m(10,\mathcal{E}_m)\equiv(Z_0^2/m)\Delta(10,\mathcal{E}_m)$; if the ion has atomic number Z_0, mass m (amu), energy per unit mass $\mathcal{E}_m\equiv E/m$ (Mev/amu), and range $R(\mathcal{E}_m)$ (mg/cm²), then its range difference $[R(10)-R(\mathcal{E}_m)]$ is given by the relation $[R(10)-R(\mathcal{E}_m)]=[m/Z_0^2][X_1(10,\mathcal{E}_m)+\Delta_m(10,\mathcal{E}_m)]$. For convenience, in addition to the values of $\Delta_m(10,\mathcal{E}_m)$ the values of $X_1(10,\mathcal{E}_m)$ also are tabulated. At ion energies intermediate to those listed in the Table the values of $X_1(10,\mathcal{E}_m)$ [defined by the relation $X_1(10,\mathcal{E}_m)\equiv R_1(10)-R_1(\mathcal{E}_m)$] can be calculated using Eq. (4), while the appropriate values of $\Delta_m(10,\mathcal{E}_m)$ can be obtained by interpolation between the tabulated values. Although the results were obtained with beams of specific isotopes (i.e., specific values of m for each Z_0), they should be applicable for other isotopes as well, provided that the correct value of m is used. Moreover, since the values of $\Delta_m(10,\mathcal{E}_m)$ for beams of Li or Be would be expected to fall between the values for He and B the range differences for Li and Be isotopes also can be found from this table with considerable accuracy. The range differences for beams of Na, Mg, and Al ions can be estimated with reasonable certainty, by noting the systematic variation of $\Delta_m(10,\mathcal{E}_m)$ with Z_0. The values given for $\Delta_m(10,\mathcal{E}_m)$ are least accurate at zero energy where their uncertainty is equivalent to a range uncertainty of $\sim\pm\frac{1}{2}$ mg/cm² or larger.

$\mathcal{E}_m$ (Mev/amu)	Δ_m X_1	He	B	C	N	O	F	Ne
11	−30.73	0	−0.02	−0.06	−0.17	−0.34	−0.60	−0.96
10.5	−15.08	0	−0.01	−0.03	−0.09	−0.18	−0.31	−0.50
10	0	0	0	0	0	0	0	0
9.5	14.50	0	0.01	0.04	0.09	0.19	0.34	0.53
9	28.42	0	0.02	0.08	0.20	0.40	0.70	1.09
8.5	41.75	0	0.03	0.13	0.31	0.63	1.09	1.69
8	54.50	0	0.05	0.18	0.44	0.88	1.51	2.34
7.5	66.63	0	0.07	0.24	0.59	1.16	1.97	3.03
7	78.18	0	0.09	0.31	0.74	1.46	2.47	3.77
6.5	89.10	0	0.12	0.40	0.94	1.80	3.01	4.57
6	99.40	0	0.15	0.49	1.15	2.17	3.60	5.44
5.5	109.08	0	0.19	0.61	1.38	2.59	4.25	6.37
5	118.12	0	0.24	0.74	1.65	3.05	4.96	7.39
4.5	126.51	0	0.31	0.90	1.96	3.57	5.75	8.49
4	134.24	0	0.38	1.08	2.32	4.15	6.62	9.70
3.5	141.29	0	0.48	1.31	2.73	4.81	7.58	11.02
3	147.65	0	0.60	1.58	3.21	5.57	8.66	12.49
2.5	153.35	0	0.79	1.96	3.82	6.44	9.89	14.13
2	158.24	0.005	1.09	2.47	4.50	7.45	11.30	16.01
1.5	162.49	0.023	1.60	3.23	5.36	8.70	13.01	18.25
1	165.97	0.053	2.54	4.54	6.49	10.31	15.19	21.10
0.5	(168.28)							
0	169.82	0.87	7.39	10.11	12.32	16.76	22.81	29.91

N^{13}, N^{14}, $\cdots$) is obtained with equal ease.

Stopping Powers

In many experimental situations the stopping power for an ion is of more interest than its range. The stopping power can be calculated from the slope of the Δ plot using Eq. (6), or alternatively, by the use of Eq. (3) with the value of γ^2 given in Eq. (10). The results of such calculations are displayed in Fig. 10. For comparison the results of Kahn[27] on the stopping power for protons in aluminum also are shown. The discontinuity in the stopping-power curves at $\mathcal{E}_m=2.657$ Mev/amu arises from the lack of agreement between the two formulas of Eq. (4) at their overlap point and is probably somewhat smaller than the uncertainty in the stopping-power curves at that point. At most energies the results for heavy ions are probably of greater accuracy than the differences between curves for neighboring ions. However, the uncertainties increase with decreasing ion energy approximately as the spread between curves increases, and the curve shape below $\mathcal{E}_m=2$ Mev/amu is of doubtful significance.

[27] D. Kahn, Phys. Rev. **90**, 503 (1953).

Effective Charge

For the purposes of the foregoing analysis the quantity γ can be regarded as nothing more than a convenient parameter with which to characterize the differences between $d\mathcal{E}_m/dX_m$ and $d\mathcal{E}_1/dX_1$. However, if the function $f(v)$ of Eq. (2) truly is independent of ion identity as assumed, then the quantity γZ_0 has a direct physical interpretation as the rms charge of the ion. Specifically, if N_Z denotes the fractional probability that the ion has charge Z (i.e., the equilibrium fraction of the ions in a monoenergetic beam passing through an absorber that have charge Z), then from the Z^2 dependence of the stopping-power formula it follows that the "effective charge" γZ_0 of the ion (i.e., the fictitious charge which would give rise to the observed rate of energy loss) is given by the relation

$$(\gamma Z_0)^2=\sum_{Z=1}^{Z_0} Z^2 N_Z. \tag{11}$$

This formula can be used to calculate the value of γ^2 from the charge state distribution. However, its validity hinges upon the assumption that $f(v)$ is independent of ion identity. Although the quantum mechanical

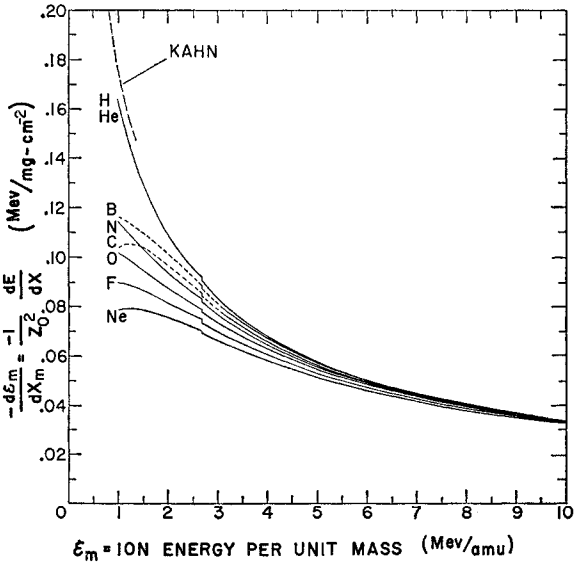

FIG. 10. Stopping power curves for heavy ions in aluminum, derived from the Δ variations of Fig. 7. The results are reduced approximately to the same scale by giving them in terms of the "universalized" measure of absorber thickness $X_m\equiv(Z_0^2/m)X$ and the ion energy per unit mass $\mathcal{E}_m\equiv E/m$. The curve for helium ions is indistinguishably different from that given for protons by Bichsel's formulas [Eq. (4)]. The discontinuity in each curve at $\mathcal{E}_m=2.657$ Mev/amu is of no physical significance, but merely reflects a disagreement between the two formulas of Eq. (4) at their joining point. The uncertainty in the stopping power is largest at low energies. For purposes of comparison the proton stopping-power curve given by Kahn (reference 27) also is shown.

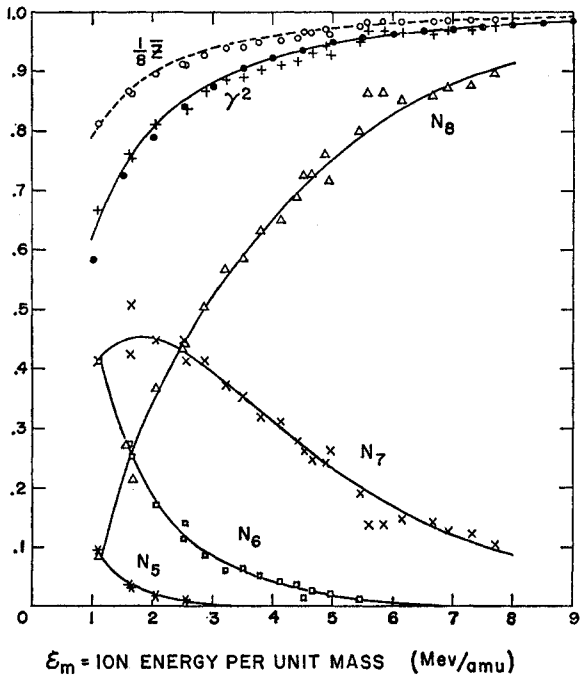

FIG. 11. The equilibrium charge state distribution, effective charge, and average charge of O^{16} ions emerging from aluminum foils as a function of emergent ion energy. The quantity N_Z is the fraction of O^{16} ions having charge Z, inferred from the relative intensities of the spectral lines. The values of γ^2 calculated from the charge state data [using Eq. (11)] are shown by the + symbols, and the corresponding values of the average charge Z are shown by the open circles. The solid circles represent the values of γ^2 deduced from the slope of the Δ plot, and the solid line shows the variation of γ^2 given by the empirical formula, Eq. (10). The dashed line is the variation of γ as given by Eq. (10). The smooth curves drawn through the points for N_8, N_7, N_6, and N_5 merely represent plausible fits to the data.

theory of Bethe[28] is in accord with this assumption, the classical theory of Bohr[29] and the more general quantum mechanical theory of Bloch[30] are not, since they give expressions for the quantity $f(v)$ which contain a logarithmic dependence on Z_{eff}. According to Williams[31] the applicability of the classical vs the quantum mechanical treatment is determined by the value of the parameter $Z_{\text{eff}}(e^2/\hbar v)$, the Bethe formula being appropriate for $Z_{\text{eff}}(e^2/\hbar v)\ll 1$ and the Bohr formula for $Z_{\text{eff}}(e^2/\hbar v)\gg 1$. In this experiment the values of $Z_{\text{eff}}(e^2/\hbar v)$ vary between $\frac{1}{4}$ and $\frac{3}{4}$ and represent a borderline case. Thus the alternative interpretation of the quantity γ^2 cannot be taken for granted. However, it can be tested, since the charge state distributions can be deduced from the densitometer plots, and the values of γ^2 calculated by means of Eq. (11) can be compared directly with the values obtained from $d\mathcal{E}_m/dX_m$.

The equilibrium distribution of charge states for O^{16} ions in aluminum, as obtained from the densitometer plots, is shown in Fig. 11. Also shown are the values of γ^2 calculated from these distributions by means of Eq. (11), the values of γ^2 obtained by means of Eq. (7) from the slope of the original dashed line fit to the Δ plot for O^{16}, and the value of γ^2 given by Eq. (10). The differences between these values of γ^2 are seen to be small, and in view of the uncertainties in the charge state distributions they are believed to be insignificant. Thus the results are consistent with the assumption that $f(v)$ is independent of ion identity.

The values of the average charge, $\bar{Z}\equiv\sum_{Z=1}^{Z_0} ZN_Z$, calculated from the charge state data, also are plotted in Fig. 11 along with the value of γ as given by Eq. (10). It is seen that the average charge is well represented by γ despite the difference in weighting. The value of γ calculated from Eq. (10) may be expected to give the average charge equally well for other ions. This result is of practical value, since the number of ions in an incident beam usually is deduced from the total charge carried by the ions, and little information is available on the average charge of heavy ions at higher energies. Work is in progress on the extraction of the charge state distributions and the straggling parameter from the densitometer plots for all ion beams studied in this experiment.

ACKNOWLEDGMENTS

The author wishes to express his gratitude to the many persons who at various times offered their facilities, equipment, assistance, advice, and encouragement. He is especially indebted to Professor R. Beringer, who designed the spectrograph magnet and Dr. M. S. Malkin, who supervised its construction, to A. F. Poulton for the precision machine work on the spectograph chamber, to Professor F. E. Steigert and his group for their generous assistance in the earlier stages of the experiment, to F. W. Martin for his help in the setup of the equipment and in the data taking, and to Dr. C. E. Anderson for many stimulating discussions.

[28] H. Bethe, Ann. Physik **5**, 325 (1930).
[29] N. Bohr, Phil. Mag. **25**, 10 (1913).
[30] F. Bloch, Ann. Physik **16**, 285 (1933).
[31] E. J. Williams, Revs. Modern Phys. **17**, 217 (1954).

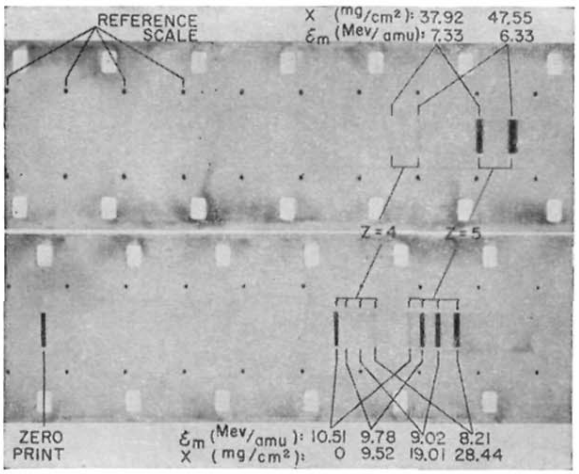

FIG. 4. Two representative film strips obtained with the apparatus of Fig. 2, showing the reference scale, several spectral lines (by multiple exposure), and a beam print made with the magnet current turned off (i.e., the "zero" of the reference scale). The incident beam is $B^{11}(4+)$, and the initial ion energy (per unit mass) is fixed at $\varepsilon_m{}^0=10.51$ Mev/amu. The spectra correspond to six different thicknesses X of absorber placed in the path of the beam. The positions of the spectral lines for $Z=4$ and $Z=5$ are indicated for each absorber thickness, along with the emergent ion energy per unit mass ($\varepsilon_m \equiv E/m$) as determined from the line position. The faint line for $Z=5$ with no absorber is explained by charge exchange occurring in the residual gas of the vacuum system, between the magnetic analyzer and the spectrograph. The almost complete conversion to $Z=5$ is expected when absorbers are used. At each energy the equilibrium charge distribution of the ions can be inferred from the relative line intensity, and the energy straggling from the linewidth.